ADVANCED FUNCTIONAL MATERIALS
www.afm-journal.de

"Ship-in-a-Bottle" Growth of Noble Metal Nanostructures

*Manda Xiao, Chunmei Zhao, Huanjun Chen, Baocheng Yang, and Jianfang Wang**

Noble metal nanostructures are grown inside hollow mesoporous silica microspheres using "ship-in-a-bottle" growth. Small Au seeds are first introduced into the interior of the hollow microspheres. Au nanorods with synthetically tunable longitudinal plasmon wavelengths and Au nanospheres are obtained through seed-mediated growth within the microspheres. The encapsulated Au nanocrystals are further coated with Pd or Pt shells. The microsphere-encapsulated bimetallic core/shell nanostructures can function as catalysts. They exhibit high catalytic performance and their stability is superior to that of the corresponding unencapsulated core/shell nanostructures in the catalytic oxidation of *o*-phenylenediamine with hydrogen peroxide. Therefore, these hollow microsphere-encapsulated metal nanostructures are promising as recoverable and efficient catalysts for various liquid-phase catalytic reactions.

1. Introduction

Porous hollow microspheres have attracted great interest in the past few decades due to their distinct characteristics such as the large void volume and structurally tunable porous shell.[1,2] The void volume can be used for the encapsulation of various guests and the porous shell allows for the rapid transport of reactants with high size selectivity. The encapsulation of functional nanoparticles inside the void further enriches the applications of porous hollow microspheres from controlled release of substances,[3–5] batteries,[6,7] water treatment,[8,9] biological sensing[10] to catalysis.[11–13]

Porous hollow microspheres carrying catalysts in the void are promising for catalysis as they provide a confined microenvironment for chemical reactions. The local concentration of reactants in the hollow microsphere can be higher than that in the surrounding environment due to the adsorption of reactant molecules in the porous shell, which leads to enhanced catalytic reaction rates.[9,14] In addition, the porous shell with predesigned permeability can strongly affect the selectivity of catalytic reactions.[15,16] Moreover, the low density of porous hollow microspheres makes them dispersible finely in solutions without sedimentation even when large amounts of catalysts are loaded.[17] They can also be easily recovered by centrifugation or filtration due to the large size of the microspheres. So far, many metal nanostructure catalysts encapsulated in hollow microspheres have been designed and utilized for heterogeneous catalytic reactions. For example, Pd nanoparticle-loaded hollow polystyrene nanospheres exhibit high activity and stability in allyl alcohol hydrogenation and Heck reaction.[17] Poly(*o*-phenylenediamine) hollow microspheres containing Au nanoparticles of controllable sizes and morphologies have been utilized for catalytic aerobic alcohol oxidation.[11] Pd nanoparticle-loaded hollow mesoporous silica nanospheres exhibit superior activity in Suzuki coupling reactions. The reaction yields reach 99.5% within 3 min.[13] In addition, shell–corona hollow microspheres that are made of block copolymers and loaded with metal nanoparticles are found to be highly efficient for a series of reactions, including hydrogenation of olefin, hydrodechlorination of chlorophenols, and aerobic oxidation of alcohols.[12,18,19]

To incorporate functional components into hollow microstructures, one feasible route is to deposit active nanoparticles onto sacrificial templating microspheres. Further growth of an outer layer on the microspheres and subsequent removal of the templates give rise to hollow microspheres encapsulating the active nanoparticles. This strategy has been applied to the preparation of several types of catalysts embedded in hollow silica and polymer microspheres.[10,13,20–22] In this approach, the deposition of nanoparticles on templating microspheres requires the functionalization of the nanoparticle surface with particular molecules. In addition, removal of templating microspheres through dissolution in solvents or thermal calcination must be carefully performed, in order not to cause aggregation and damage to the contained nanoparticles. Such hybrid microstructures can also be obtained in a one-step fashion, where the formation of hollow microstructures and encapsulation of metal nanoparticles are processed simultaneously. Examples include the production of iron oxide nanoparticles encapsulated in hollow silica microspheres through an evaporation-induced self-assembly process and the hydrothermal transformation of guest-adsorbed solid silica microspheres into hollow silica microspheres holding the guest.[6,23] The one-step method is only suitable for some particular material combinations. Moreover, the loading of active materials can also be realized by a "ship-in-a-bottle" approach, where molecular or ionic precursors are first infiltrated into the void of preformed hollow microstructures and subsequently converted into active

M. D. Xiao, Dr. H. J. Chen, Prof. J. F. Wang
Department of Physics
The Chinese University of Hong Kong
Shatin, Hong Kong SAR, China
E-mail: jfwang@phy.cuhk.edu.hk
C. M. Zhao, Prof. B. C. Yang
Institute of Nanostructured Functional Materials
Huanghe Science and Technology College
Zhengzhou, Henan 450006, China

DOI: 10.1002/adfm.201200941

species. Such an approach can be applied to various types of hollow microstructures and different encapsulated materials, including metal, metal oxide nanoparticles as well as polymers and proteins,[24–29] although the morphological control of encapsulated materials is hardly achieved.[11] In addition, removal of templates in the ship-in-a-bottle approach occurs before the growth of active species in the void. The multistep surface modification and adsorption required for the deposition of pre-formed nanoparticles on templating microspheres are not needed.

Here we report on the ship-in-a-bottle growth of noble metal nanostructures inside hollow mesoporous silica microspheres (HMSMSs). Au nanoparticle seeds are first prepared in the void of the HMSMSs by reducing dissolved metal salts in the presence of the microspheres. Au nanorods with controllable longitudinal plasmon resonance wavelengths and Au nanospheres are then prepared inside the microspheres from the seeds via seed-mediated growth. The composition of the noble metal nanostructures inside the microspheres is further varied by coating Pd or Pt layers onto the encapsulated Au nanocrystals. The microspheres carrying bimetallic core/shell nanostructures can act as efficient catalysts for the oxidation of *o*-phenylenediamine (OPDA) with H_2O_2. Control experiments show that these microsphere-protected metal nanostructure catalysts have superior recyclability in comparison to the unprotected metal nanostructure catalysts. Our microsphere-encapsulated metal nanostructures can therefore be potentially utilized as recoverable and efficient catalysts for various liquid-phase catalytic reactions.

2. Results and Discussion

The HMSMSs were prepared through a templated growth method as we described before.[30] Nearly monodisperse polystyrene microspheres with an average diameter of 1.32 ± 0.02 μm were used as templates. The scanning electron microscopy (SEM) image is shown in **Figure 1**A. The coating of mesostructured silica shells on the polystyrene microspheres was realized through the hydrolysis and condensation of tetraethyl orthosilicate in the presence of cetyltrimethylammonium bromide (CTAB) as the structure-directing agent. Calcination of the obtained core/shell microspheres produced the HMSMSs, which have an average diameter of 1.37 ± 0.02 μm and shell thickness of 54 ± 4 nm, as estimated from SEM and transmission electron microscopy (TEM) images (Figure 1B,C). The mesoporous nature of the silica shell has been verified in our previous study.[30] After calcination, the HMSMSs were subjected to hydrothermal treatment at 100 °C for 2 h to make them more hydrophilic. The high-angle annular dark-field scanning transmission electron microscopy (HAADF-STEM) imaging of a single HMSMS reveals that in addition to mesopores, there are also many larger pores on the silica shell. The larger pores have an average diameter of 9 ± 3 nm (Figure 1D,E). They are possibly formed during the calcination and hydrothermal treatment.

The HMSMSs were then utilized for the ship-in-a-bottle growth of noble metal nanostructures. We first prepared Au nanospheres and nanorods inside the HMSMSs, since they have found a wide range of applications in optics and biotechnology owing to their attractive plasmonic properties.[31–34] For the growth, the HMSMSs were first dispersed in a mixture solution composed of $HAuCl_4$ and CTAB. The addition of $NaBH_4$ into the mixture solution produced small Au nanoparticle seeds both inside and outside the HMSMSs. The HMSMSs containing the Au seeds can be readily separated from the free Au seeds in the solution by centrifugation at a low speed. They were thereafter mixed with the standard growth solution for the preparation of Au nanospheres and nanorods. **Figure 2** shows the morphologies of the Au nanospheres and nanorods grown within the HMSMSs. The smooth outer surface of the microspheres suggests that the metal nanocrystals are encapsulated within the microspheres instead of being adsorbed on the outer surface (Figure 2B,E). The encapsulation of the metal nanocrystals is further verified by a TEM image adjusted to have a higher contrast (Figure S1A, Supporting Information), showing clearly the smooth outer surface of a single HMSMS containing Au nanorods inside, and by comparing the SEM images (Figure S1B,C, Supporting Information) of a single HMSMS containing Au nanorods inside and one with Au nanorods adsorbed on the outer surface.[30] The presence of the Au nanospheres and nanorods can be clearly differentiated in the magnified TEM images of the single HMSMSs (Figure 2C,F). The Au nanospheres have an average diameter of 18 ± 2 nm, while the Au nanorods have an average diameter and length of 13 ± 2 nm and 48 ± 3 nm, respectively. The HMSMSs containing the Au nanorods exhibit a strong extinction peak around 825 nm, which is ascribed to the longitudinal plasmon resonance of the Au nanorods (Figure 2G). The extinction signal from 470 to 640 nm is contributed by both the transverse plasmon resonance of the Au nanorods and the plasmon resonance of a small fraction of Au nanospheres coformed during the preparation. The size of the encapsulated Au nanorods and thus their longitudinal plasmon resonance wavelength can also be varied by changing the volume of the added seed solution (Figure S2, Supporting Information). In comparison, the HMSMSs containing the Au nanospheres exhibit only one peak around 530 nm. The rising background towards the

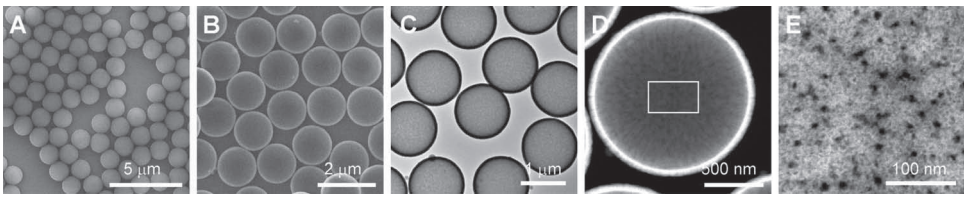

Figure 1. Morphology and structure of the HMSMSs. A) SEM image of the polystyrene microspheres. B,C) SEM and TEM images of the HMSMSs. D) HAADF-STEM image of a single HMSMS. E) Zoomed-in HAADF-STEM image of the boxed area in (D).

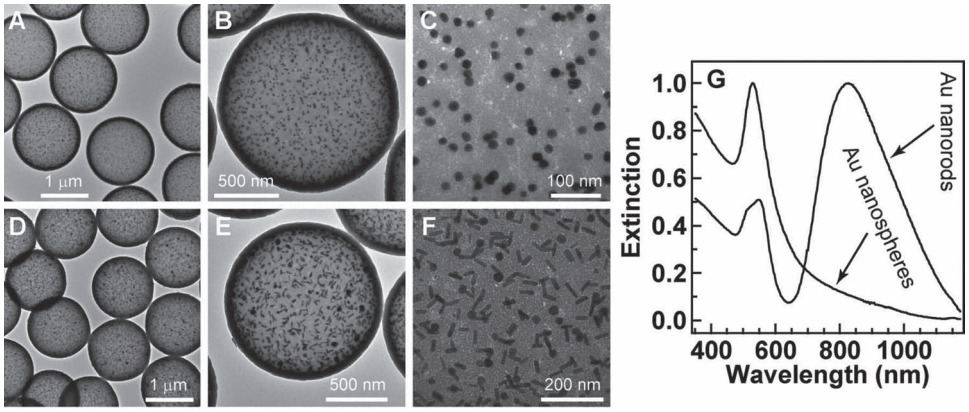

Figure 2. HMSMS-encapsulated Au nanospheres and nanorods. Au nanospheres grown inside the HMSMSs: A) low-magnification TEM image; B) TEM image of a single HMSMS; and C) zoomed-in TEM image of the HMSMS shown in (B). D–F) Corresponding images for the Au nanorods grown inside the HMSMSs by use of 50 μL of the seed solution. G) Normalized extinction spectra of the aqueous dispersions of the Au nanospheres and nanorods grown inside the HMSMSs.

shorter wavelength on the extinction spectra of both samples is due to the increasing scattering from the HMSMSs. The yields of the Au nanospheres and nanorods inside the HMSMSs were estimated by comparing the extinction peak intensities of the supernatant solutions and the precipitates redispersed in water at the same volume (Figure S3, Supporting Information). For the Au nanorods, the longitudinal plasmon peaks were considered. The obtained yields of the Au nanospheres and nanorods in the HMSMSs are 95% and 90%, respectively. The presence of small amounts of the Au nanospheres and nanorods in the supernatant solutions is because the seeds for the growth of the Au nanospheres and nanorods are smaller than the larger pores on the HMSMSs. Some seeds can get out of the HMSMSs during the growth process. We also performed TEM imaging on the Au nanostructures that were produced under the same conditions and collected from the supernatant solutions (Figure S4, Supporting Information). The nanostructures also have a sphere or rod shape. Their average sizes are 21 ± 3 nm and 13 ± 2 nm $\times$ 45 ± 5 nm for the Au nanospheres and nanorods, respectively. Therefore, the shapes and sizes of the single-component Au nanostructures are nearly the same inside and outside the HMSMSs. Because the seed-mediated growth of Au nanorods and nanospheres relies on the cooperative interactions of the Au seeds, the Au complex ions, the reducing agent, and the surfactant molecules, the successful growth of Au nanorods and nanospheres inside the HMSMSs suggests that the transfer of the molecular species across the mesoporous silica shell is facile. This result is in contrast with what has been observed in the previous studies of the diffusion properties of molecular species in mesoporous materials, where the diffusion of molecules in the mesopores is found to be limited by the defects in the mesoporous structure.[35,36] We reason that the larger pores on the silica shell can provide effective channels for the rapid exchange of the solutes inside and outside the hollow microspheres.

Although small Au nanoparticles have been found to exhibit high catalytic activities for some chemical reactions, the catalytic applications of Au nanoparticles have been less developed than those of other noble metals, such as palladium and platinum.[37–39] We therefore utilized wet chemistry to coat the encapsulated Au nanocrystals with a layer of palladium or platinum. Such heterometallic core/shell nanostructures not only enable a wider range of applications in plasmonics and catalysis but also offer enhanced catalytic stabilities in comparison to monometallic nanostructures, as evidenced previously.[40–49] **Figure 3** shows the morphology of the Au nanorod core/Pd shell nanostructures grown within the HMSMSs. The starting HMSMS-encapsulated Au nanorod sample is the same as that shown in Figure 2D–F. A few nanoparticles were seen to be adsorbed on the outer surface of the HMSMSs, which is ascribed to the self-nucleation of Pd nanoparticles during the reduction of H_2PdCl_4 (Figure 3A,B). The zoomed-in TEM image on a single HMSMS reveals that the Pd-coated nanostructures retain the rod shape (Figure 3C). In order to better examine their

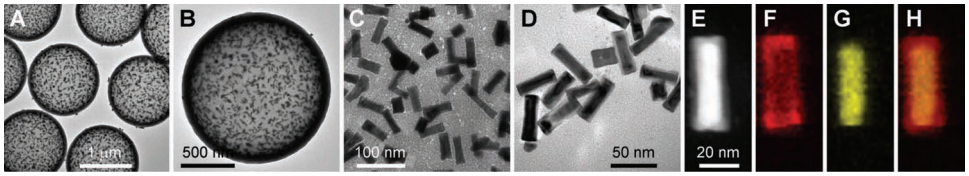

Figure 3. HMSMS-encapsulated Au nanorod core/Pd shell nanostructures. A) low-magnification TEM image; B) TEM image of a single HMSMS; and C) zoomed-in TEM image of the HMSMS shown in (B). D) TEM image of the core/shell nanostructures released by dissolving the HMSMSs with a NaOH solution. E) HAADF-STEM image of a released core/shell nanostructure. F) Elemental map of palladium on the nanostructure shown in (E). G) Corresponding elemental map of gold. H) Merged elemental map.

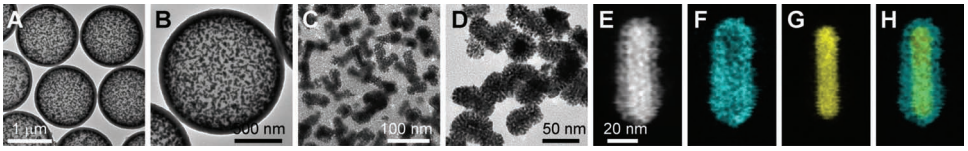

Figure 4. HMSMS-encapsulated Au nanorod core/Pt shell nanostructures: A) low-magnification TEM image; B) TEM image of a single HMSMS; and C) zoomed-in TEM image of the HMSMS shown in (B). D) TEM image of the core/shell nanostructures released by dissolving the HMSMSs with a NaOH solution. E) HAADF-STEM image of a released core/shell nanostructure. F) Elemental map of platinum on the nanostructure shown in (E). G) Corresponding elemental map of gold. H) Merged elemental map. The starting HMSMS-encapsulated Au nanorod sample is the same as that shown in Figure 2D–F.

internal structure, the core/shell nanostructures were released by dissolving the HMSMSs with a NaOH solution (Figure 3D). The Pd layer was found to be conformally coated on the Au nanorods with a layer thickness of ≈3 nm, which is also indicated with the HAADF-STEM image and elemental maps of a single Au nanorod core/Pd shell nanostructure (Figure 3E–H). Pd coating was also similarly made on the Au nanospheres contained in the HMSMSs. TEM characterizations show that each Au nanosphere is completely embedded in a Pd shell, but the thickness of the Pd shell within a core/shell nanostructure is nonuniform (Figure S5, Supporting Information). As a result, the Au nanosphere core/Pd shell nanostructures are irregularly shaped and have a large size distribution.

The preparation of Pt-coated Au nanorods inside the HMSMSs was similar to that of the Pd-coated Au nanorods. A difference is that the reduction of H_2PtCl_6 with ascorbic acid was much slower than that of H_2PdCl_4. The slower reduction led to the minimization of the self-nucleation of Pt nanoparticles in the growth solution. As a result, the outer surface of the HMSMSs containing Pt-coated Au nanorods remains smooth (**Figure 4**A,B). In contrast to the conformal coating of palladium on the Au nanocrystal surface, the coating of platinum on the Au nanorods incorporated in the HMSMSs produced a porous shell of ≈7 nm in thickness. The porous Pt shell is composed of many small Pt nanoparticles, as shown in Figure 4D–H. The formation of the Pt nanoparticle shell is attributed to the stronger bond between the shell atoms than that between the shell and substrate atoms.[40,46] The coating of platinum onto the Au nanospheres contained in the HMSMSs yielded similar results (Figure S6, Supporting Information). In addition, both Pd and Pt coating resulted in strong damping of the plasmon resonances of the original Au nanospheres and nanorods, as indicated by the extinction spectra (Figure S7, Supporting Information). The plasmon damping arises from the much larger imaginary dielectric constants of palladium and platinum than that of gold. Moreover, during the growth of the core/shell nanostructures, the supernatant solutions are clear without any color, suggesting that almost all of the nanostructures are present inside the HMSMSs. This is because the Au cores are much larger than the pores on the HMSMSs. They cannot get out of the HMSMSs during the growth process.

The catalytic performance of the HMSMS-encapsulated metal nanostructures were evaluated using the liquid-phase oxidation of OPDA with H_2O_2 at room temperature as the model catalytic reaction. The Au nanorod core/Pt shell nanostructures contained in the HMSMSs were employed as the catalyst (**Figure 5**A), because previous studies have shown that the reaction can be accelerated by Pt nanoparticles due to their peroxidase-like activities.[50] OPDA has no absorption in the spectral region above 350 nm. The oxidation of OPDA yields a yellow product of 2,3-diaminophenazine (DAP) with an absorption peak around 420 nm. The reaction process can therefore be monitored by recording the absorption spectra of the reaction solution as a function of the reaction time. Figure 5B shows the time-dependent absorption spectra of the reaction solution. The increasing background towards the shorter wavelength is contributed by the extinction of the Au nanorod core/Pt shell nanostructures and the scattering of the HMSMSs. The absorption peak at 420 nm increases gradually in intensity. The peak intensity becomes nearly saturated at a maximal value at 30 min after the addition of the catalyst, suggesting that the reaction has reached equilibrium. Using the reported molar absorption coefficient,

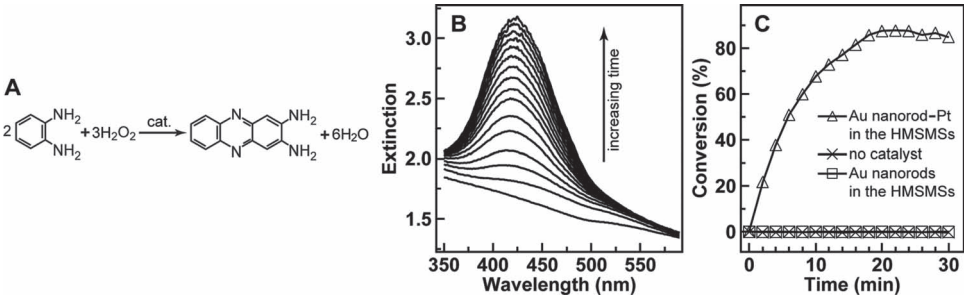

Figure 5. Catalytic oxidation of OPDA to DAP with the HMSMS-encapsulated Au nanorod core/Pt shell nanostructures. A) Reaction equation. B) Time-dependent absorption spectra of the reaction solution. The time interval between the neighboring spectra is 2 min. C) Conversion percentages of OPDA as functions of the reaction time in the presence of the HMSMS-encapsulated Au nanorod–Pt shell nanostructures (triangles), the HMSMS-encapsulated Au nanorods (squares), or in the absence of the metal nanostructures (crosses).

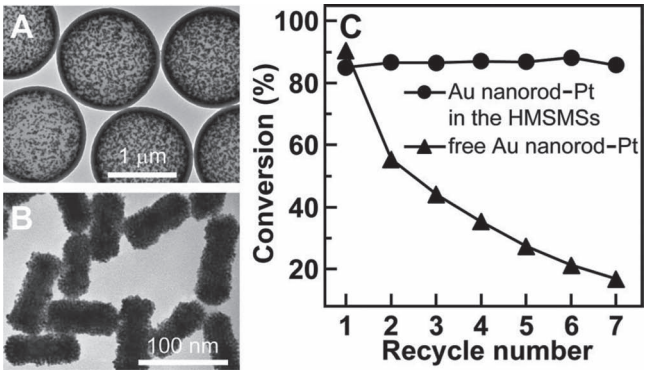

Figure 6. Catalytic recyclability of the HMSMS-encapsulated Au nanorod core/Pt shell nanostructures. A) TEM image of the HMSMS-encapsulated Au nanorod core/Pt shell nanostructures. B) TEM image of the free Au nanorod core/Pt shell nanostructures. C) Conversion percentages of OPDA versus the recycle number with the encapsulated (circles) and free (triangles) core/shell nanostructures as the catalysts.

$\varepsilon_{418\ nm}$ = 16982 M^{-1} cm^{-1}, of the neutral form of DAP,[51] we can estimate that ≈85% of OPDA has been transformed into DAP during the first 30 min in the presence of the HMSMS-encapsulated Au nanorod core/Pt shell nanostructures. In contrast, no reaction was observed in the presence of the HMSMS-encapsulated Au nanorods or in the absence of metal nanostructure catalysts (Figure 5C).

The stability of catalysts is an important issue in their practical applications. In order to test the catalytic stability of the HMSMs-encapsulated metal nanostructure catalysts, the catalytic oxidation reaction was successively carried out. At the end of each cycle, the HMSMS-encapsulated Au nanorod core/Pt shell nanostructures (**Figure 6**A) were separated from the previous reaction solution by centrifugation and redispersed in a fresh reaction solution. As shown in Figure 6C, the conversion percentage of OPDA remains barely unchanged even after seven cycles of the reaction. This result demonstrates the excellent stability of the HMSMS-encapsulated Au nanorod core/Pt shell nanostructures in the catalytic oxidation reaction. For comparison, the free, unencapsulated Au nanorod core/Pt shell nanostructure sample (Figure 6B) was also ascertained for its catalytic stability. Its concentration was adjusted so that the conversion percentage of OPDA at 30 min in the first cycle was about the same as that obtained using the microsphere-encapsulated metal nanostructure sample as the catalyst (Figure S8, Supporting Information). Under this condition, the Pt amount in the free core/shell nanostructures is 96% of that in the HMSMS-encapsulated core/shell nanostructures. The conversion percentage of OPDA using the free nanostructure catalyst drops consecutively during recycling. It decreases to only 20% by the seventh cycle. The reduction in the catalytic performance of the free nanostructure catalyst during recycling is mainly caused by the loss of the nanostructures during separation by centrifugation. Therefore, the encapsulation of the metal nanostructures within the hollow microspheres greatly facilitates the recovery of the nanostructures from the reaction solution and enhances their long-term catalytic stability during recycling.

3. Conclusions

In summary, HMSMSs containing Au nanocrystals in the void were prepared through a "ship-in-bottle" procedure. By changing the growth composition, either Au nanorods with different longitudinal plasmon resonance wavelengths or Au nanospheres were formed within the HMSMSs. Bimetallic Au core/Pd shell and Au core/Pt shell nanostructures were further prepared using the encapsulated Au nanocrystals as seeds. The formed Pd shell on the Au nanocrystals was dense and in intimate contact, while the coated Pt shell was discontinuous and composed of many small nanoparticles. Compared to the corresponding unencapsulated metal nanostructures, the microsphere-encapsulated Au nanorod core/Pt shell nanostructures exhibited both high catalytic performance and superior stability in the oxidation reaction of OPDA with H_2O_2. Our strategy for the preparation of microsphere-encapsulated metal nanostructure catalysts through the ship-in-a-bottle preparation can be generally extended to different types of microspheres and various nanoparticle catalysts. The hollow microsphere-encapsulated metal nanostructure catalysts also look promising as effective and recyclable catalysts in liquid-phase catalytic reactions.

4. Experimental Section

Preparation of the HMSMSs: The HMSMSs were produced by growing mesostructured silica shells on pre-prepared polystyrene microspheres according to our described procedure[30] with slight modification of the reaction compositions. For the preparation of the polystyrene microspheres, styrene (20 mL), poly(vinyl pyrrolidone) (6 g, M_w = 55000), 2,2′-azobis(2-methylpropionitrile) (0.2 g), ethanol (95 mL), and water (3 mL) were added to a 250-mL, three-necked, round-bottom flask equipped with a reflux condenser and a nitrogen gas inlet. The air in the flask was replaced by nitrogen, and the mixture was kept under nitrogen until the polymerization was finished. The dispersion polymerization was carried out at 70 °C for 24 h, and the stirring rate was set at 120 rpm. The resultant solution was filtered, rinsed with deionized water and dried under vacuum. To prepare the HMSMSs, the obtained polystyrene microspheres (2 g) were first dispersed in a mixture containing CTAB (1.92 g), ethanol (128 mL), water (100 mL), and $NH_3{\cdot}H_2O$ (1.6 mL, 28 wt%) under ultrasonication. The mixture solution was subsequently stirred for 10 min and tetraethyl orthosilicate (3.44 mL) was then quickly added, followed by additional stirring for 3 min. The mixture was thereafter kept undisturbed overnight. The product was collected by filtration and then calcined at 550 °C for 6 h with a ramp rate of 1 °C min^{-1} to remove polystyrene and CTAB templates. To make the HMSMSs more hydrophilic, the HMSMSs (0.1 g) were dispersed in H_2O (80 mL) under ultrasonication. The resultant mixture was transferred to a 100-mL, Teflon-lined autoclave and heated at 100 °C for 2 h. After being cooled down to room temperature, the HMSMSs were collected by filtration.

Growth of the Au Nanospheres and Nanorods in the HMSMSs: Au nanoparticle seeds were first grown inside the HMSMSs. To prepare the seed solution, the HMSMSs (50 mg) were dispersed in a mixture solution of $HAuCl_4$ (0.25 mL, 0.01 M) and CTAB (9.75 mL, 0.1 M) under ultrasonication. A freshly prepared, ice-cold aqueous $NaBH_4$ solution (0.6 mL, 0.01 M) was then added into the mixture solution under vigorous magnetic stirring. The resultant solution was stirred for 2 min and then kept at room temperature for 2 h before use. The seed-contained HMSMSs were subsequently separated by centrifugation (1500 *g*, 5 min), washed with an aqueous CTAB solution (0.1 M), and finally redispersed in an aqueous CTAB solution (1 mL, 0.1 M). The

growth solution of the Au nanorods was made by first mixing together $HAuCl_4$ (0.5 mL, 0.01 M), $AgNO_3$ (0.1 mL, 0.01 M), CTAB (10 mL, 0.1 M) and HCl (0.2 mL, 1.0 M). A freshly prepared aqueous ascorbic acid solution (0.08 mL, 0.1 M) was then added. After the resultant solution was mixed by gently inverting the closed container repeatedly, different amounts of the seed-contained HMSMS solutions (50, 100, 200, 600 μL) were added. The reaction mixture was subjected to gentle inversion for 10 s and then left undisturbed for at least 6 h. The growth solution of the Au nanospheres was composed of $HAuCl_4$ (0.25 mL, 0.01 M), CTAB (10 mL, 0.1 M), HCl (0.2 mL, 1.0 M), and ascorbic acid (0.04 mL, 0.1 M). After the seed-contained HMSMS solution (100 μL) was added, the growth solution was kept undisturbed. The HMSMSs containing the Au nanorods and nanospheres were separated by centrifugation (1500 *g*, 5 min), washed with aqueous CTAB solutions (0.1 M), and finally redispersed in water (10 mL).

Growth of the Au Core/Pd Shell and Au Core/Pt Shell Nanostructures within the HMSMSs: The Au nanospheres and nanorods within the HMSMSs were utilized as seeds for the growth of the core/shell nanostructures. The HMSMSs containing the Au nanospheres and nanorods that were prepared from the addition of 100 μL of the seed solution were chosen. To coat palladium on the Au nanocrystals inside the HMSMSs, the HMSMS-encapsulated Au nanocrystal solution (5 mL) was mixed with CTAB (1 mL, 0.1 M), H_2PdCl_4 (0.25 mL, 0.01 M), and ascorbic acid (0.25 mL, 0.1 M). The resultant solution was kept undisturbed at room temperature for 5 h. For Pt coating, the HMSMS-encapsulated Au nanocrystal solution (5 mL) was mixed with H_2PtCl_6 (0.25 mL, 0.01 M) and ascorbic acid (0.25 mL, 0.1 M). The resultant solution was placed in an oven set at 65 °C for 1 h. The HMSMSs containing the Au core/Pd shell or Au core/Pt shell nanostructures were separated by centrifugation (1500 *g*, 5 min), washed with aqueous CTAB solutions (0.1 M), and finally redispersed in water (5 mL).

Growth of the Au Nanorod Core/Pt Shell Nanostructures for the Control Experiment: The Au nanorods were obtained from NanoSeedz and prepared according to our previous method.[52] The as-prepared Au nanorods were precipitated by centrifugation (6300 *g*, 10 min), washed once with water (2.5 mL) by centrifugation (6300 *g*, 10 min), and then redispersed in water (5 mL). To this solution was added a mixture solution of CTAB (0.1 mL, 0.1 M), H_2PtCl_6 (0.05 mL, 0.01 M), and ascorbic acid (0.5 mL, 0.1 M). The resultant solution was placed in an oven set at 65 °C for 3 h. The obtained Au nanorod core/Pt shell nanostructures were separated by centrifugation (6300 *g*, 5 min), washed with aqueous CTAB solutions (0.1 M), and finally redispersed in water (2.5 mL).

Catalytic Oxidation of OPDA: For the catalytic oxidation of OPDA, the HMSMS-encapsulated Au nanorod–Pt shell nanostructure solution (0.25 mL) or the unencapsulated Au nanorod–Pt shell nanostructure solution (0.6 mL) was mixed with an aqueous solution of OPDA (5 μL, 0.1 M), H_2O_2 (50 μL, 30 wt%), and H_2O (1 mL) in a plastic cuvette with gentle agitation. The resultant solution was then transferred into the sample holder of a spectrophotometer. The reaction progress at room temperature, without stirring, was monitored by taking absorption spectra at certain time intervals. For testing the catalyst stability, a CTAB solution (0.1 mL, 0.1 M) was added to the reaction solution at the end of each cycle to stabilize the nanostructures. The microsphere-encapsulated catalysts or the control catalysts were separated by centrifugation (1500 *g*, 5 min for the microsphere-encapsulated catalysts, 6300 *g*, 10 min for the control catalysts) and redispersed into a fresh mixture solution of the reactants.

Release of the Encapsulated Metal Nanostructures from the HMSMSs: The HMSMS-encapsulated Au core/Pd shell or Au core/Pt shell nanostructure solution (1 mL) was mixed with a CTAB solution (0.1 mL, 0.1 M), followed by the addition of a NaOH solution (0.2 mL, 5 M). The resultant solution was kept undisturbed for 5 h to ensure complete dissolution of the silica microspheres. The released core/shell nanostructures were separated by centrifugation (1500 *g*, 5 min) and redispersed in H_2O for TEM characterizations.

Instrumentation: Extinction and absorption spectra were measured on a Hitachi U-3501 UV/visible/NIR spectrophotometer with cuvettes that had an optical path length of 0.5 cm. SEM images were taken on an FEI Quanta 400 FEG microscope. TEM imaging was performed on an FEI CM120 microscope at 120 kV. Elemental mapping and HAADF-STEM characterizations were carried out on a FEI Tecnai F20 microscope equipped with an Oxford energy-dispersive X-ray analysis system.

Supporting Information

Supporting Information is available from the Wiley Online Library or from the author.

Acknowledgements

This work was supported by NSFC/RGC Joint Research Scheme (Ref. No.: N_CUHK465/09, Project Code: 2900339), Hong Kong RGC (GRF Grant, Ref. No.: CUHK403211, Project Code: 2130277 and Special Equipment Grant, Ref. No.: SEG_CUHK06).

Received: April 3, 2012
Revised: May 21, 2012
Published online: June 29, 2012

[1] J. Liu, F. Liu, K. Gao, J. S. Wu, D. F. Xue, *J. Mater. Chem.* **2009**, *19*, 6073.
[2] J. Hu, M. Chen, X. S. Fang, L. M. Wu, *Chem. Soc. Rev.* **2011**, *40*, 5472.
[3] A. G. Skirtach, P. Karageorgiev, B. G. De Geest, N. Pazos-Perez, D. Braun, G. B. Sukhorukov, *Adv. Mater.* **2008**, *20*, 506.
[4] A. G. Skirtach, P. Karageorgiev, M. F. Bédard, G. B. Sukhorukov, H. Möhwald, *J. Am. Chem. Soc.* **2008**, *130*, 11572.
[5] M. F. Bédard, B. G. De Geest, A. G. Skirtach, H. Möhwald, G. B. Sukhorukov, *Adv. Colloid Interface Sci.* **2010**, *158*, 2.
[6] W.-M. Zhang, J.-S. Hu, Y.-G. Guo, S.-F. Zheng, L.-S. Zhong, W.-G. Song, L.-J. Wan, *Adv. Mater.* **2008**, *20*, 1160.
[7] S. J. Ding, J. S. Chen, G. G. Qi, X. N. Duan, Z. Y. Wang, E. P. Giannelis, L. A. Archer, X. W. Lou, *J. Am. Chem. Soc.* **2011**, *133*, 21.
[8] D. P. Wang, H. C. Zeng, *Chem. Mater.* **2011**, *23*, 4886.
[9] Y. Yamada, M. Mizutani, T. Nakamura, K. Yano, *Chem. Mater.* **2010**, *22*, 1695.
[10] M. Sanles-Sobrido, W. Exner, L. Rodríguez-Lorenzo, B. Rodríguez-González, M. A. Correa-Duarte, R. A. Álvarez-Puebla, L. M. Liz-Marzán, *J. Am. Chem. Soc.* **2009**, *131*, 2699.
[11] J. Han, Y. Liu, R. Guo, *Adv. Funct. Mater.* **2009**, *19*, 1112.
[12] Y. Lan, L. Yang, M. C. Zhang, W. Q. Zhang, S. N. Wang, *ACS Appl. Mater. Interfaces* **2010**, *2*, 127.
[13] Z. Chen, Z.-M. Cui, F. Niu, L. Jiang, W.-G. Song, *Chem. Commun.* **2010**, *46*, 6524.
[14] S. M. Leeder, M. R. Gagné, *J. Am. Chem. Soc.* **2003**, *125*, 9048.
[15] L. Pan, H. M. Liu, X. G. Lei, X. Y. Huang, D. H. Olson, N. J. Turro, Jing Li, *Angew. Chem. Int. Ed.* **2003**, *42*, 542.
[16] E. Kockrick, T. Lescouet, E. V. Kudrik, A. B. Sorokin, D. Farrusseng, *Chem. Commun.* **2011**, *47*, 1562.
[17] S. D. Miao, C. L. Zhang, Z. M. Liu, B. X. Han, Y. Xie, S. J. Ding, Z. Z. Yang, *J. Phys. Chem. C* **2008**, *112*, 774.
[18] Y. Lan, M. C. Zhang, W. Q. Zhang, L. Yang, *Chem. Eur. J.* **2009**, *15*, 3670.
[19] L. Yang, M. C. Zhang, Y. Lan, W. Q. Zhang, *New J. Chem.* **2010**, *34*, 1355.
[20] X. W. Lou, C. L. Yuan, E. Rhoades, Q. Zhang, L. A. Archer, *Adv. Funct. Mater.* **2006**, *16*, 1679.

[21] G. D. Moon, U. Jeong, *Chem. Mater.* **2008**, *20*, 3003.
[22] L. Li, J. Ding, J. M. Xue, *Chem. Mater.* **2009**, *21*, 3629.
[23] T. H. Zheng, J. B. Pang, G. Tan, J. B. He, G. L. McPherson, Y. F. Lu, V. T. John, J. J. Zhan, *Langmuir* **2007**, *23*, 5143.
[24] L. Dähne, S. Leporatti, E. Donath, H. Möhwald, *J. Am. Chem. Soc.* **2001**, *123*, 5431.
[25] Y. Zhou, Q. M. Ji, Y. Shimizu, N. Koshizaki, T. Shimizu, *J. Phys. Chem. C* **2008**, *112*, 18412.
[26] W. S. Choi, H. Y. Koo, D.-Y. Kim, *Langmuir* **2008**, *24*, 4633.
[27] T. Shiomi, T. Tsunoda, A. Kawai, S. Matsuura, F. Mizukami, K. Sakaguchi, *Small* **2009**, *5*, 67.
[28] A. D. Price, A. N. Zelikin, K. L. Wark, F. Caruso, *Adv. Mater.* **2010**, *22*, 720.
[29] J. P. Deng, Y. Yu, S. Dun, W. T. Yang, *J. Phys. Chem. B* **2010**, *114*, 2593.
[30] M. D. Xiao, H. J. Chen, T. Ming, L. Shao, J. F. Wang, *ACS Nano* **2010**, *4*, 6565.
[31] P. K. Jain, X. H. Huang, I. H. El-Sayed, M. A. El-Sayed, *Acc. Chem. Res.* **2008**, *41*, 1578.
[32] C. J. Murphy, A. M. Gole, J. W. Stone, P. N. Sisco, A. M. Alkilany, E. C. Goldsmith, S. C. Baxter, *Acc. Chem. Res.* **2008**, *41*, 1721.
[33] R. Wilson, *Chem. Soc. Rev.* **2008**, *37*, 2028.
[34] T. K. Sau, A. L. Rogach, F. Jäckel, T. A. Klar, J. Feldmann, *Adv. Mater.* **2010**, *22*, 1805.
[35] A. Zürner, J. Kirstein, M. Döblinger, C. Bräuchle, T. Bein, *Nature* **2007**, *450*, 705.
[36] F. Furtado, P. Galvosas, M. Gonçalves, F.-D. Kopinke, S. Naumov, F. Rodríguez-Reinoso, U. Roland, R. Valiullin, J. Kärger, *J. Am. Chem. Soc.* **2011**, *133*, 2437.
[37] L. X. Yin, J. Liebscher, *Chem. Rev.* **2007**, *107*, 133.
[38] Y. H. Bing, H. S. Liu, L. Zhang, D. Ghosh, J. J. Zhang, *Chem. Soc. Rev.* **2010**, *39*, 2184.
[39] A. Balanta, C. Godard, C. Claver, *Chem. Soc. Rev.* **2011**, *40*, 4973.
[40] F.-R. Fan, D.-Y. Liu, Y.-F. Wu, S. Duan, Z.-X. Xie, Z.-Y. Jiang, Z.-Q. Tian, *J. Am. Chem. Soc.* **2008**, *130*, 6949.
[41] Y. W. Lee, M. Kim, Z. H. Kim, S. W. Han, *J. Am. Chem. Soc.* **2009**, *131*, 17036.
[42] L. Wang, Y. Yamauchi, *J. Am. Chem. Soc.* **2010**, *132*, 13636.
[43] C.-L. Lu, K. S. Prasad, H.-L. Wu, J. A. Ho, M. H. Huang, *J. Am. Chem. Soc.* **2010**, *132*, 14546.
[44] Y. Yu, Q. B. Zhang, B. Liu, J. Y. Lee, *J. Am. Chem. Soc.* **2010**, *132*, 18258.
[45] W. W. He, X. C. Wu, J. B. Liu, K. Zhang, W. G. Chu, L. L. Feng, X. N. Hu, W. Y. Zhou, S. S. Xie, *Langmuir* **2010**, *26*, 4443.
[46] F. Wang, L.-D. Sun, W. Feng, H. J. Chen, M. H. Yeung, J. F. Wang, C.-H. Yan, *Small* **2010**, *6*, 2566.
[47] F. Wang, C. H. Li, L.-D. Sun, H. S. Wu, T. Ming, J. F. Wang, J. C. Yu, C.-H. Yan, *J. Am. Chem. Soc.* **2011**, *133*, 1106.
[48] M. L. Tang, N. Liu, J. A. Dionne, A. P. Alivisatos, *J. Am. Chem. Soc.* **2011**, *133*, 13220.
[49] C.-W. Yang, K. Chanda, P.-H. Lin, Y.-N. Wang, C.-W. Liao, M. H. Huang, *J. Am. Chem. Soc.* **2011**, *133*, 19993.
[50] W. W. He, Y. Liu, J. S. Yuan, J.-J. Yin, X. C. Wu, X. N. Hu, K. Zhang, J. B. Liu, C. Y. Chen, Y. L. Ji, Y. T. Guo, *Biomaterials* **2011**, *32*, 1139.
[51] K. C. Brown, J. F. Corbett, N. P. Loveless, *Spectrochim. Acta* **1979**, *35A*, 421.
[52] W. H. Ni, X. S. Kou, Z. Yang, J. F. Wang, *ACS Nano* **2008**, *2*, 677.